Journal of Materials Chemistry

Cite this: *J. Mater. Chem.*, 2012, **22**, 19113

www.rsc.org/materials

PAPER

Polypropylene/layered double hydroxide nanocomposites

Qiang Wang,[a] Xi Zhang,[b] Chengle J. Wang,[a] Jiahua Zhu,[b] Zhanhu Guo[b] and Dermot O'Hare*[a]

Received 30th May 2012, Accepted 25th July 2012
DOI: 10.1039/c2jm33493c

We report a novel synthesis method for the preparation of polypropylene/layered double hydroxide (PP/LDH) nanocomposites, in which LDH nanosheets, $[Mg_2Al(OH)_6](DDS)\cdot 2H_2O$ (Mg–Al–DDS), were prepared using a one-step reverse microemulsion method. PP/LDH nanocomposites were prepared by direct mixing of the obtained LDH nanosheets with PP in xylene at 140 °C. Loadings of the LDH in PP of 0.5, 1.0, 1.5, 2.0, 4.0, 8.0 and 16.0 wt% were investigated. The results indicate that the LDH nanosheets were highly dispersed in PP and this dramatically improves the performance of the nanocomposites at very low LDH loadings (*e.g.* 1.0 wt%). In particular, the thermal stability, melting transition, recrystallisation behavior, and rheological properties of the PP/LDH nanocomposites were evaluated. The thermal stability ($T_{0.5}$) of the pure PP was increased from 336 to 384 °C by 1.0 wt% addition of the Mg–Al–DDS nanosheets. At 1.0 wt% loading the melting temperature (T_m) and the recrystallisation temperature (T_c) of PP were also increased by 2.5 and 6.7 °C respectively. The nanocomposites showed decreased G' and G'' when the LDH nanoplatetet loading is low (<2.0 wt%). With 0–2.0 wt% of LDHs, both G' and G'' decreased with the increase of LDH loading. While on increasing the LDH loading from 2.0 wt% to 16.0 wt% both the storage modulus (G') and loss modulus (G'') gradually increased. At a 16.0 wt% LDH loading, the rheological response changes and the elastic solid-like behavior is observed, with only a limited reduction in G' at low frequency. For the PP/LDH nanocomposites containing 0.5–4.0 wt% LDH, tan δ decreases monotonously with increasing frequency (w). Above 8.0 wt% LDH loading, tan δ starts to show three different stages: rubbery, viscoelastic and a glassy state. These results demonstrate that the reverse microemulsion method is a simple and efficient approach for the one-step synthesis of LDH nanosheets for use in the synthesis of polymer/LDH nanocomposites with enhanced thermal, rheological and mechanical properties.

1. Introduction

In recent years, polymer/LDH nanocomposites have attracted considerable interest in the field of materials chemistry.[1–6] Since high mechanical, optical, thermal and rheological properties are rarely present in pure polymers or micro-scale composites, these hybrids are seen to have a wide range of applications such as organoceramics, biomaterials, electrical, and mechanical materials.[7–13] It is believed that the bulk property improvements are due to the small size together with the high aspect ratio of the filler particles, and its homogeneous dispersion on the nanoscale within the polymeric matrix.[14] In addition, since the chemical composition of LDHs can be precisely controlled, these materials should find applications in areas such as microelectronic and medical materials where the chemical purity is often a critical requirement. To date, numerous types of polymer/LDH nanocomposites have been reported, which include polypropylene (PP)/Mg–Al–LDH,[15,16] PP/Zn–Al–LDH,[17] PP/Co–Al–LDH,[18] low density polyethylene (LDPE)/Mg–Al–LDH,[19] linear low density polyethylene (LLDPE)/Zn–Al–LDH,[20] high density polyethylene (HDPE)/Zn–Al–LDH,[21] poly(methyl methacrylate) (PMMA)/Zn–Al–LDH,[22] PMMA/Mg–Al–LDH,[23] polyvinyl chloride (PVC)/Mg–Al–LDH,[24] PVC/Zn–Al–LDH,[25] PVC/Mg–Al–Ce–LDH,[26] PVC/Mg–Cu–Al–LDH,[27] polystyrene (PS)/Mg–Al–LDH, PS/Co–Al–LDH, PS/Ni–Al–LDH, PS/Cu–Al–LDH, PS/Cu–Fe–LDH, and PS/Cu–Cr–LDH,[28] ethylene vinyl acetate (EVA)/Mg–Al–LDH, EVA/Zn–Al–LDH,[29] polylactic acid (PLA)/Zn–Al–LDH,[30] polyamide (PL)/Co–Al–LDH,[31,32] Epoxy (EP)/Mg–Al–LDH,[33] poly(propylene carbonate) (PPC)/Mg–Al–LDH,[34] nylon 6/Mg–Al–LDH,[35] polyethylene oxide (PEO)/Mg–Al–LDH,[36] polymethacrylate (PMA)/Zn–Al–LDH,[37] and polystyrenesulfonate (PSS)/Zn–Al–LDH.[38] The polymers PP and PE are the most widely used in the preparation of nanocomposites due to their ready availability and relatively low cost.[39,40] Mg–Al, Zn–Al, and Zn–Mg–Al LDHs are the most preferred fillers, since these white materials will not cause any unwanted colour to the mother polymers.[29] However, most importantly the ultimate performance

[a]*Chemistry Research Laboratory, Department of Chemistry, University of Oxford, 12 Mansfield Road, Oxford, OX1 3TA, UK. E-mail: dermot.ohare@chem.ox.ac.uk; Tel: +44 (0)1865 272686*
[b]*Integrated Composites Laboratory, Dan F Smith Department of Chemical Engineering, Lamar University, Beaumont, TX 77710, USA*

of any LDH/polymer nanocomposites strongly depends on the degree of dispersion and the compatibility of LDHs in the polymer matrices.[21]

Although there are a number of approaches for the preparation of nanocomposites, the route involving the exfoliation of the inorganic component is the one that usually attracts the most interest since this tends to result in a better dispersion of an inorganic material in the polymer matrix and enhanced properties as compared to, for example, intercalated nanocomposites.[6,41] However, since LDH layers possess a high charge density (*ca.* 3 mequiv. per gram) the strong interlayer electrostatic interactions make the exfoliation of LDHs much more difficult.[42] In addition, pristine LDHs are not suitable for the penetration of giant polymer chains or chain segments into their gallery space unless their interlayer separation is significantly increased. Accordingly, the intercalation of macromolecules in LDHs involves either the organic modification of the LDH to expand the basal spacing and/or chemical modification of the polymer to graft anions into the polymers.[20]

We and others have been exploring the routes to preparing colloidal dispersions of LDH nanosheets followed by simple mixing with a polymer to obtain nanocomposites.[5,43,44] However, we believe a much more useful method would be to develop a simple (one step) synthesis of LDH nanosheets which could then be used directly to synthesise polymer/LDH nanocomposites.[45]

The reverse microemulsion method has been widely used for controlling the size and shape of inorganic nanocrystals.[46–49] Our group has developed an attractive approach for using a reverse microemulsion to control the nucleation and growth of rigid LDH nanosheets. In the reverse microemulsion system, the anionic surfactants dissolved in organic solvents form spheroidal reverse micelles with the hydrophobic chains pointing out into the oil phase. A remarkable function of these systems is the initial isolation of a space. When water (or aqueous solution) is added, the micelles swell with water droplets entrapped at the polar cores that are formed by the hydrophilic heads of the surfactants. Then, under controlled reaction conditions, the LDH nanosheets are induced to form within the limited space.[45,50–52] With this method, several LDHs have been synthesised, including Mg–Al,[45,50,51] Co–Al,[52] Ni–Al,[53] Ca–Al,[54] and Zn–Co–Fe.[55]

Here we report the first direct synthesis of a polymer/layered double hydroxide (PP/LDH) nanocomposite by the addition of LDH nanosheets synthesised using a reverse microemulsion method.

2. Experimental section

2.1 Synthesis

Synthesis of $[Mg_2Al(OH)_6](DDS)\cdot 2H_2O$ (Mg–Al–DDS LDH) nanosheets. A metal precursor solution (A) was prepared by dissolving 18.43 g $Mg(NO_3)_2\cdot 6H_2O$ and 9 g $Al(NO_3)_3\cdot 9H_2O$ in 30 ml degassed and de-ionised (DI) water. The base solution (B) was prepared by dissolving 6.97 g $NaNO_3$ and 4.8 g NaOH in 30 ml deionised H_2O. The DDS intercalated Mg–Al LDH nanosheets were prepared by a reverse microemulsion method.[45,50–52] 1.8 g NaDDS $\{CH_3(CH_2)_{11}OSO_3Na\}$, 1.9 g 1-butanol, and 2.15 g solution A were added to 130 ml isooctane to obtain a transparent solution (C). 1.8 g NaDDS, 4 g 1-butanol and 1.55 g of solution B were added to 120 ml isooctane to obtain a transparent solution (D). If solution D is not transparent, more 1-butanol was added until the solution turned transparent. Then solution D was added drop-wise into solution C with magnetic stirring. Finally, the mixture was aged at 75 °C for 24 h. After aging, LDH nanosheets were separated by centrifugation (3750 rpm) and washed first with H_2O/ethanol (1 : 1) twice, then with acetone twice. After washing, the obtained LDH slurry was directly used for the preparation of PP/LDH nanocomposites.

Synthesis of PP/LDH nanocomposites. 5 g PP, the LDH slurry prepared above and 100 ml xylene were charged into a 250 ml round bottom flask. The amount of LDH added to the PP corresponds to 0.5, 1.0, 1.5, 2.0, 4.0, 8.0 and 16.0 wt%, respectively. The mixture was refluxed at approximately 140 °C for 2 h. After the reflux process was completed, a hot xylene solution containing dissolved PP and highly dispersed LDH nanosheets was poured into 100 ml hexane (also called a solvent extraction method).[56,57] This results in the precipitation of the PP/LDH nanocomposites as a white solid which was collected by filtration and dried in a vacuum.

2.2 Characterization

X-ray diffraction (XRD). XRD patterns were recorded on a PANalytical X'Pert Pro instrument in reflection mode with Cu Kα radiation. The accelerating voltage was set at 40 kV with 40 mA current ($\lambda = 1.542$ Å) at 0.01° s^{-1} from 1° to 70° with a slit size of 1/32 degree.

Fourier transform infrared (FT-IR) spectroscopy. FT-IR spectra were recorded on a Bio-Rad FTS 6000 FTIR Spectrometer equipped with a DuraSamplIR II diamond accessory in attenuated total reflectance (ATR) mode in the range of 400–4000 cm^{-1}; 100 scans at 4 cm^{-1} resolution were collected. The strong absorption in the range 2500–1667 cm^{-1} was from the DuraSamplIR II diamond surface.

Transmission electron microscopy (TEM). TEM analysis was performed on a JEOL 2100 microscope with an accelerating voltage of 400 kV. LDH nanosheets were dispersed in ethanol with sonication and then cast onto copper TEM grids coated with a Formvar film.

Scanning electron microscopy (SEM) and energy dispersive X-ray spectrometry (EDS). SEM and SEM-EDS analyses were performed on a JEOL JSM 6100 scanning microscope with an accelerating voltage of 20 kV. A Mg–Al–DDS LDH bulk sample was spread on carbon tape adhered to an SEM stage. Before observation, the samples were sputter coated with a thin Platinum layer to prevent charging and to improve the image quality.

2.3 Property measurements

Thermal stability behavior. The thermal stability of neat PP and its nanocomposites was studied by thermal gravimetric analysis (TGA, Netzsch), which was carried out with a heating rate of 10 °C min^{-1} and an air flow rate of 20 ml min^{-1} from 25 to 600 °C.

Recrystallisation and melting behavior. The recrystallisation and melting behaviors of neat PP and nanocomposites were analysed by a TA Instrument Q200 differential scanning calorimeter (DSC). Experiments were run on samples of about 10 mg. Each sample was first heated from room temperature to 220 °C with a heating rate of 10 °C min^{-1} to remove the thermal history, cooled to 40 °C at a rate of 10 °C min^{-1}, and then reheated to 220 °C at a rate of 10 °C min^{-1} to determine the melt temperature. The experiments were carried out at a nitrogen flow rate of 50 ml min^{-1}.

Rheological behavior. The melt rheological behavior of neat PP and the nanocomposites were studied using a TA Instruments AR 2000ex Rheometer. An environmental test chamber (ETC) steel parallel-plate geometry (25 mm in diameter) was used to perform the measurement at 200 °C, with dynamic oscillation frequency sweeping from 100 to 0.1 Hz in the linear viscoelastic (LVE) range (strain 1%) under a nitrogen atmosphere to prevent the oxidation of PP.

2.4 Simulation of powder XRD patterns

The simulation studies of the powder X-ray diffraction patterns of Mg–Al–DDS were carried out using the Fortran programme DIFFaX.[58] Within the DIFFaX formalism, a crystalline solid is treated as a stacking of layers, which are interconnected by a stacking operation. The PXRD pattern is simulated by integrating the diffraction intensities layer by layer. The $3R_1$ stacking sequence was chosen for Mg–Al–DDS LDH and the stacking direction was defined along the *c*-axis. The interlayer distance was set as 3 nm. Since we are interested in the thickness of platelet LDHs, the width of the *a*, *b*-plane was set as infinite. The powder XRD patterns were simulated by integrating the diffraction intensities layer by layer.

3 Results and discussion

3.1 Synthesis and characterization of Mg–Al–DDS nanosheets

A reverse microemulsion is a ternary system containing water (aqueous solutions of salts for synthetic purposes), oil, and surfactants. In our synthesis, isooctane was used as the oil phase, NaDDS was used as the surfactant, and 1-butanol was employed as a co-surfactant. The aqueous phase which contains the ions (Mg^{2+}, Al^{3+}, OH^-) required for the growth of the LDH crystallites are dispersed in the oil phase to form droplets surrounded by DDS groups. The Brownian motion of the micellar aggregates will lead to continuous collisions among the aggregates and consequently the exchange of ions between the droplets entrapped by the surfactant shells. The Al^{3+} and Mg^{2+} cations from metal precursor solution A react with the OH^- anions from the basic solution B, forming LDH nuclei during the process of coalescence and decoalescence between the water pools when the two systems are mixed together. Upon heating at elevated temperatures, the LDH nuclei grow into larger LDH nanocrystals.[52] The schematic synthesis process using a reverse microemulsion method is presented in Fig. 1. According to our previous work, the water/surfactant molar ratio (w) is the key parameter that controls the final size of the LDH phases. For instance, when $w = 12$, LDH nanosheets with a uniform 14 Å monolayer thickness could be synthesised.[45] We report herein the synthesis of Mg–Al–DDS LDH nanosheets with $w = 12$ as an additive for the preparation of PP/LDH nanocomposites in a simple one step procedure.

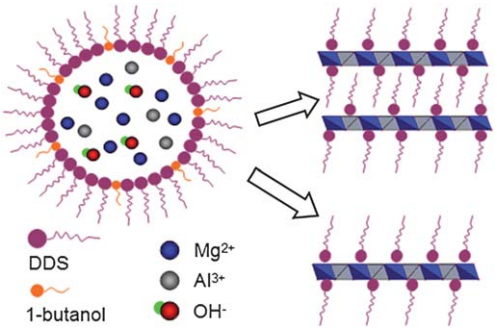

Fig. 1 Schematic representation of the nucleation and growth of LDH nanosheets in a reverse microemulsion.

The nanoplatelet $[Mg_2Al(OH)_6](DDS)\cdot 2H_2O$ (Mg–Al–DDS) LDH prepared in an isooctane, NaDDS and 1-butanol reverse microemulsion was initially characterised by FTIR analysis, as shown in Fig. 2. The –OH stretch in the brucite-like layers appeared at around 3468 cm^{-1}; the vibration of angular deformation of H_2O molecules was seen at 1628 cm^{-1}; and the Al–O and Mg–O vibrations in the brucite-like layers were found at around 679 cm^{-1}.[59–61] The interlayer anion DDS can also be identified. The absorbances at 2922 and 2850 cm^{-1} can be attributed to the antisymmetric and symmetric V_{CH} modes from the dodecyl groups, and absorbances at *ca.* 1200 and 1055 cm^{-1} are assignable to the S=O stretching mode of the sulfate groups. In addition, a small absorbance appears at 1466 cm^{-1} together with two very weak signals at 1421 and 1357 cm^{-1} which can be attributed to the CH_2 scissoring, CH_3 asymmetrical bending and symmetrical bending from the long dodecyl chains.[52]

The powder XRD for the Mg–Al–DDS LDH is shown in Fig. 3. Broad Bragg reflections indexed as (003), (006), and (009) were observed at $2\theta = 2.93°$, 6.63°, and 10.11° respectively. The interlayer distance can be calculated as 30 Å, indicating the successful intercalation of the DDS anions. The XRD patterns in the region $2\theta = 30$–60° show two low intensity reflections, which

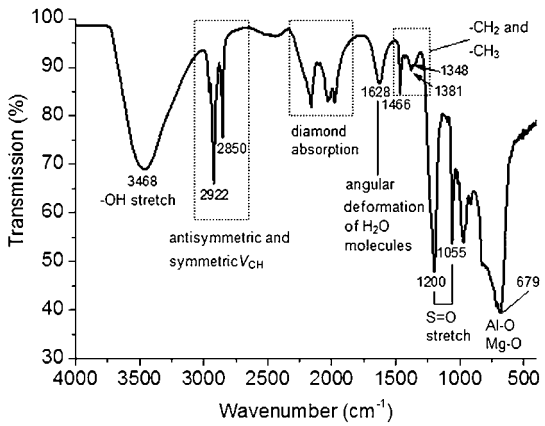

Fig. 2 FTIR analysis of a Mg–Al–DDS LDH nanoplatelet synthesised by the reverse microemulsion method.

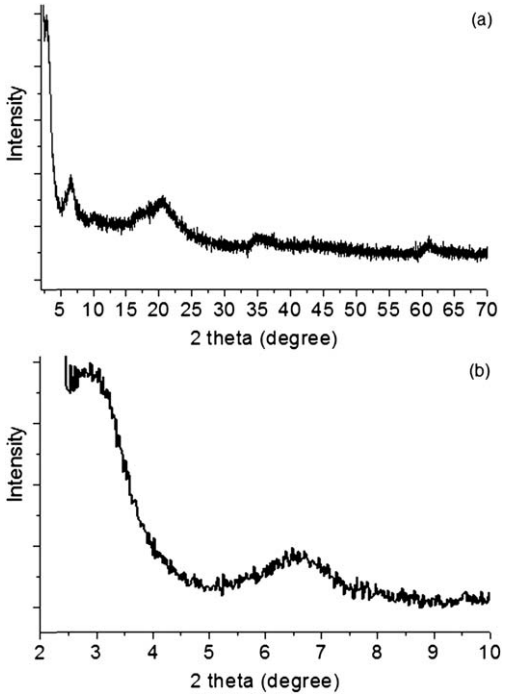

Fig. 3 XRD of the Mg–Al–DDS LDH synthesised by the reverse microemulsion method.

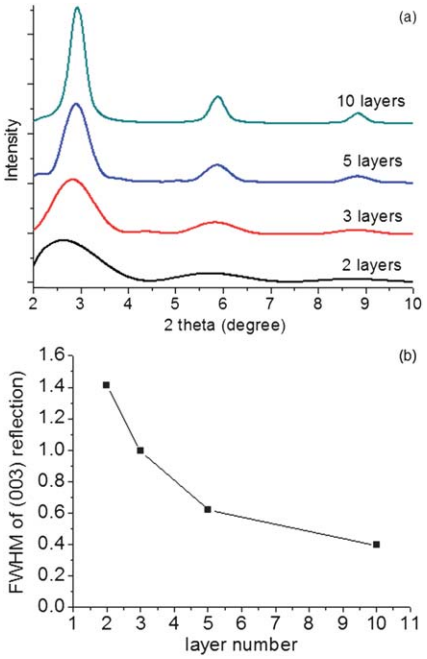

Fig. 4 (a) Simulated XRD patterns using DiFFAX of an Mg–Al–DDS LDH with layer numbers from 2 to 10. (b) The FWHM of (003) reflection as a function of layer number.

can be indexed as the nonbasal plane Bragg reflections, (012) and (110) of a hexagonal unit cell $a = b = 2d_{110} = 3.04$ Å. In addition, there is a broad feature observed at a 2θ value of around 20°, which is absent in both nitrate- and sulfate-intercalated LDHs. We tentatively attributed this feature to X-ray scattering of locally ordered carbon chains in the intercalated DDS.[62,63] The crystalline domain length derived from the 00*l* Bragg reflection line widths must be related to the thickness or stacking in the platelet samples. In order to have a convenient way to estimate the thickness of platelet LDHs using XRD data, a simulation of the X-ray diffraction patterns of a model Mg–Al–DDS structure was carried out using the DIFFaX program. Fig. 4(a) illustrates the influence of the number of stacking layers on the observed XRD patterns, while keeping the width of the *a*, *b*-plane infinite. All the Bragg reflections are broader and have a lower intensity when the number of stacking layers decreases. The position of the (00*l*) reflections shift to a lower angle when the stacking number is below 5. This is typical for nanoparticles when the number of repetitive units in a crystal is too small to be considered as long-range order relative to the atomic size. A plot of the full width at half maximum (FWHM) of the (003) Bragg reflection *versus* layer number is shown in Fig. 4(b). It shows an exponential relationship between these two factors. The thickness of the as-synthesised nanoplatelet LDHs can be estimated from this plot. The measured FWHM of our synthesised Mg–Al–DDS nanoplatets is 1.52°, which corresponds to 1–2 layers (60 Å) according to the simulation. Application of the Scherrer equation would suggest that the crystalline domain length along the *c*-axis is *ca.* 50 Å, which is consistent with the simulation result.

Our previous atomic force microscopy (AFM) indicated that very thin LDH nanosheets can be obtained using the reverse microemulsion method.[45] This was examined by further XRD analysis. After washing with ethanol/water and acetone, the LDH slurry was re-dispersed in ethanol with a concentration of *ca.* 3 mg ml^{-1}. The LDH–ethanol mixture solution was then dropped onto a glass slide and dried at 25 °C. Another three samples were prepared by repeating the above action for 2, 5, and

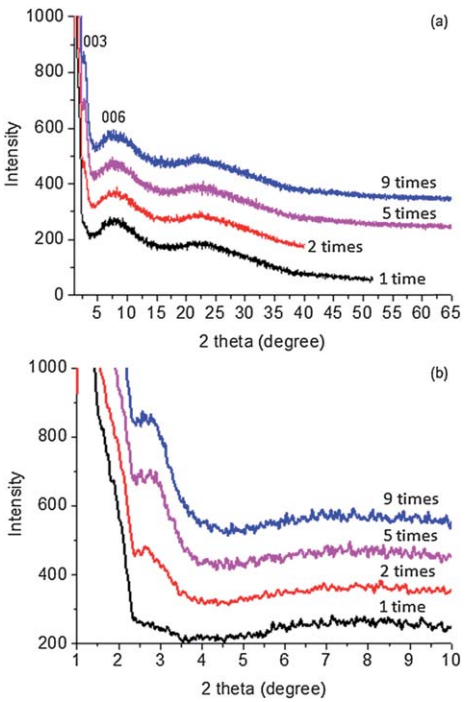

Fig. 5 XRD patterns of Mg–Al–DDS LDH nanosheets deposited on glass plates for 1, 2, 5, and 9 times.

9 times, respectively. Fig. 5(a) shows that only 00*l* Bragg reflections were observed for all four samples. The absence of reflections other than those that can be indexed as 00*l* reflections indicates that the deposited LDH platelets are highly oriented parallel to the surface of the glass slide. The (003) Bragg reflection has a low intensity from the sample using one deposition of droplets, and the reflection intensity gradually increased with repeated depositions, suggesting the building up of LDH nanosheets (Fig. 5(b)). The broad reflection at *ca.* 22° is associated with the glass slide support. A similar result was observed for delaminated LDH–glycine in formamide.[64]

The Mg–Al–DDS LDH nanosheets were further characterised by TEM and SEM. The TEM image in Fig. 6(a) clearly shows LDH platelets lying flat on the substrate, with some platelets overlapping on the edge. Furthermore, particles can often be seen through another because of the very thin nature of the platelets. Fig. 6(b) shows the SEM image of the as-synthesised Mg–Al–DDS LDH. It can be seen that the LDH nanosheets severely aggregated after drying, forming very big particles of several tens of micrometers. This clearly indicates that in order to have a good dispersion of LDH nanosheets within the polymer matrix, LDH nanosheets should be introduced into polymers before any drying step. In this work, a PP/LDH nanocomposite was prepared by a solvent mixing method using xylene as the solvent. After being washed and separated by centrifugation, the LDH nanosheet suspension was directly dispersed in xylene. Due to the intercalation with DDS, the LDH nanosheets behave as hydrophobic particles and so are highly dispersed in xylene solution. Nanocomposites were then prepared by dissolving PP in the LDH/xylene suspension at 140 °C for 2 h, followed by pouring into hexane to induce rapid precipitation.

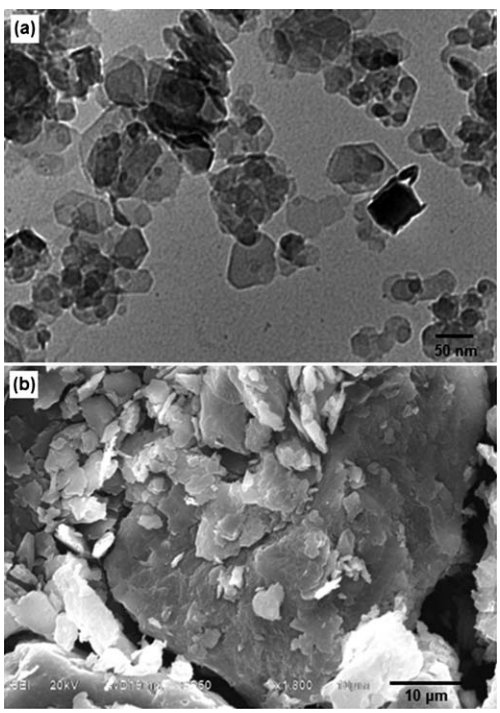

Fig. 6 (a) TEM and (b) SEM images of Mg–Al–DDS LDH synthesized by the reverse microemulsion method.

3.2 Characterization of PP/LDH nanocomposites

The PP/Mg–Al–DDS nanocomposites were initially characterised by powder XRD (Fig. 7). When the LDH loading in the polymer is lower than 2.0 wt%, a (003) Bragg reflection is observed at a very low angle of 1.87°, corresponding to an interlayer distance of *ca.* 4.7 nm. This value is much larger than the interlayer distance (3.0 nm) in bulk Mg–Al–DDS, suggesting that the Mg–Al–DDS LDH galleries are expanded by the insertion of polymer molecules. However, upon increase of LDH loading in the PP, another Bragg reflection at *ca.* 2.93° appears, this is attributed to the existence of bulk Mg–Al–DDS LDH nanoplatelets. This result suggests that in order to have a maximum dispersion of the LDH nanosheets within the PP matrix, the loading should be less than 2.0 wt%. The XRD data suggest that any higher LDH loadings will lead to the aggregation of LDH nanosheets and the formation of larger LDH agglomerates

Fig. 8 and 9 show the SEM images of PP/Mg–Al–DDS nanocomposites with the LDH loadings of 0, 1.0, 4.0, 8.0, and 16.0 wt%. Spherical particles were formed for all the samples, which is caused by the rapid precipitation of the polymer composite from hexane. For all the nanocomposite samples, aggregated LDH particles are rarely observed, which can be attributed to the ultrafine LDH particles and their good dispersion within the PP matrix. It is interesting to see that the size of the spheres decreased with the increase of LDH loadings (Fig. 10). For instance, with 0 and 1.0 wt% of LDH, the average particle size is 60 and 25 μm, respectively; while with 4.0, 8.0 and 16.0 wt% of LDH, the average particle size greatly decreased to 15, 6 and 4 μm, respectively. This result suggests that the LDH nanosheets may work as the nucleation seed during the rapid precipitation of the nanocomposites from hexane solution.[65] The degree of dispersion of the LDH in the PP was further characterised using SEM-EDS mapping (Fig. 11). The EDS spectrum showed emission from Mg, Al and S which derive solely from the Mg–Al–DDS LDH in the nanocomposite samples (Fig. 11(b)) The Mg/Al ratio is 2.1, close to the value (2.3) of the bulk nanoplatelet LDH. Fig. 11(c) and (d) show the elemental mapping for Mg and S, indicating that the LDHs are evenly distributed in the polymer nanocomposites.

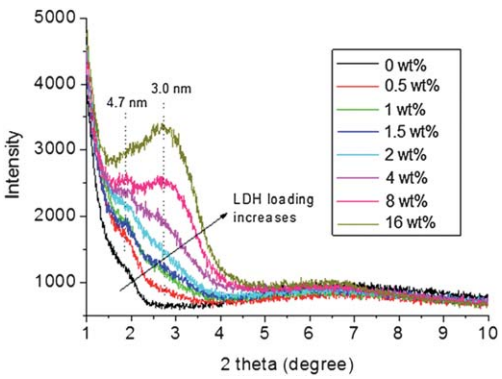

Fig. 7 Powder XRD data for PP/Mg–Al–DDS nanocomposites containing different LDH loadings (pure PP, 0.5 wt%, 1.0 wt%, 1.5 wt%, 2.0 wt%, 4.0 wt%, 8.0 wt%, and 16.0 wt%).

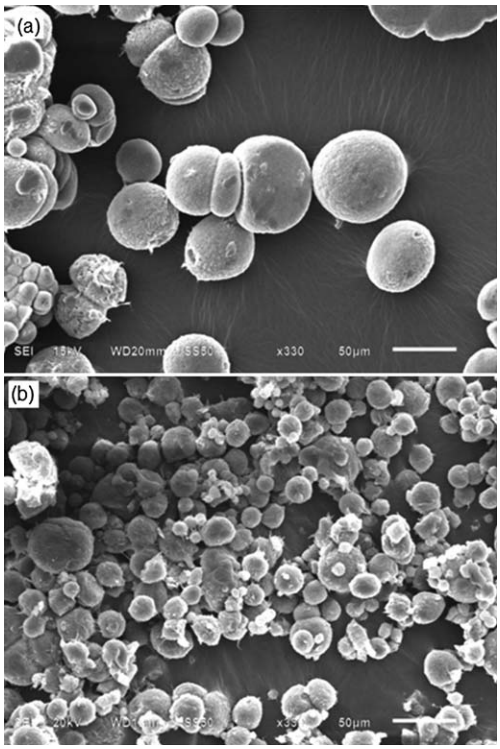

Fig. 8 SEM images of (a) pure PP and (b) 1.0 wt% PP/Mg–Al–DDS nanocomposites.

3.3 Performance tests of PP/LDH nanocomposites

The thermal stability of PP/Mg–Al–DDS nanocomposites with various LDH loadings was tested using thermogravimetric analysis (TGA) in air (Fig. 12). The 50% weight loss temperature ($T_{0.5}$) data are summarised in Fig. 12(b). It indicates that the thermal stability of the Mg–Al–DDS LDH loaded PP is higher than that of the pure PP. While increasing the LDH loadings, $T_{0.5}$ first increased from 336 °C (0 wt%) to 384 °C (1.0 wt%), and then gradually decreased to 340 °C (16.0 wt%). 1.0 wt% was determined as the optimal LDH loading, with which $T_{0.5}$ was increased by 48 °C compared to the pure PP. Similar results were also observed in other polymer/nanofiller nanocomposites.[56,66,67] Gilman and Kashiwagi[68] suggested that the barrier properties of the polymer nanocomposites, which include both thermal barrier and transport barrier, are responsible for the observed thermal property enhancement. However, there is still a significant effect on the thermal properties even when the nanoparticle loading is too low to form the barrier.[69] Zhu *et al.*[70] studied PS/clay and PS/graphite nanocomposites and suggested that the structural nanoparticles act as the operative site to trap the radicals. However, the agglomerated nanoparticles will have a little effect on the thermal stability. This is probably the reason why $T_{0.5}$ first increased with the increase of LDH loading and then decreased with excessive loadings.

The melting and recrystallisation behaviors of PP and the PP/LDH nanocomposites are very important when considering downstream processing. The melting and recrystallisation events were studied by DSC (Table 1). PP is a semicrystalline polymer and the final properties of PP based composites in engineering applications are critically dependent on the extent of crystallinity

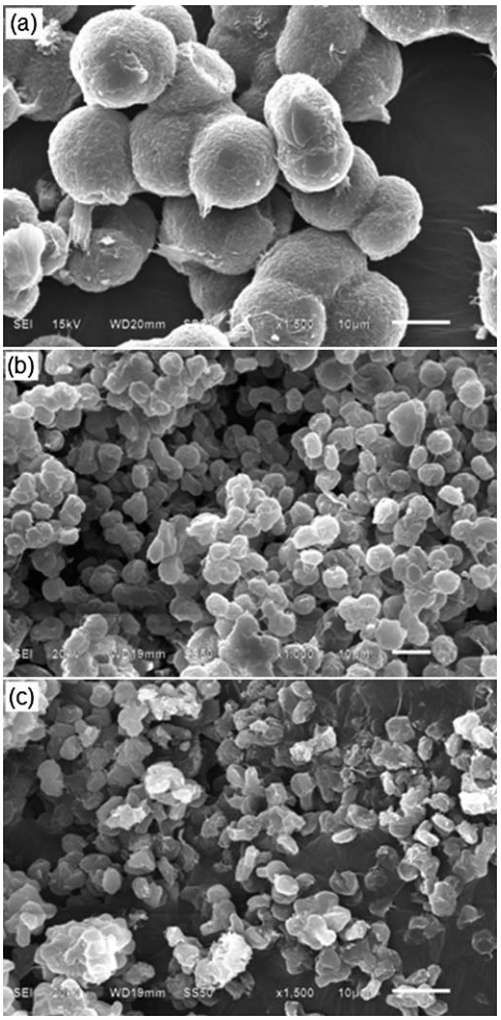

Fig. 9 SEM images of (a) 4.0 wt%, (b) 8.0 wt%, and (c) 16.0 wt% PP/Mg–Al–DDS nanocomposites.

which in turn depends on the processing conditions.[71] To remove the heat history effects induced by the prior hot press on the thermal properties, the DSC curves were recorded on the first cooling and second heating processes. After introducing LDHs, both the melting temperature (T_m) and the recrystallisation temperature (T_c) increased. For example, with 1.0 wt% loading,

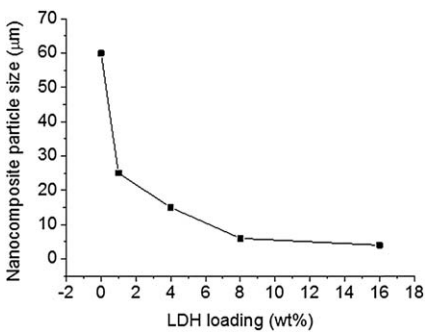

Fig. 10 The effect of LDH loading on the observed particle size of PP/Mg–Al–DDS nanocomposites.

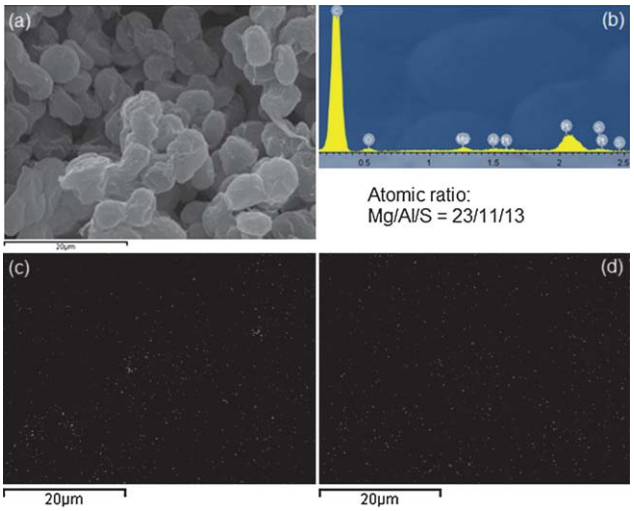

Fig. 11 (a) SEM image, (b) EDS elemental analysis, (c) Mg mapping, and (d) S mapping of 8.0 wt% PP/Mg–Al–DDS LDH nanocomposites.

T_m and T_c increase by 2.5 and 6.7 °C, respectively. However, further increase in the LDH loadings did not cause significant differences in both T_m and T_c. The crystallinity fraction (X_c) of the pure PP and the PP/LDH nanocomposites was determined by eqn (1), where the crystallinity heat of the pure crystalline PP (ΔH_c^0) was assumed to be 146.5 J g^{-1}.[71,72] At 1.0–8.0 wt% loadings, all the nanocomposites exhibited an significantly enhanced X_c by *ca.* 6.9–10.8% compared to the pure PP. When the loading is above optimum (16.0 wt%), the X_c drops to just a 3.1% increase.

$$X_c = \frac{\Delta H_c}{\Delta H_c^0} \times 100 \quad (1)$$

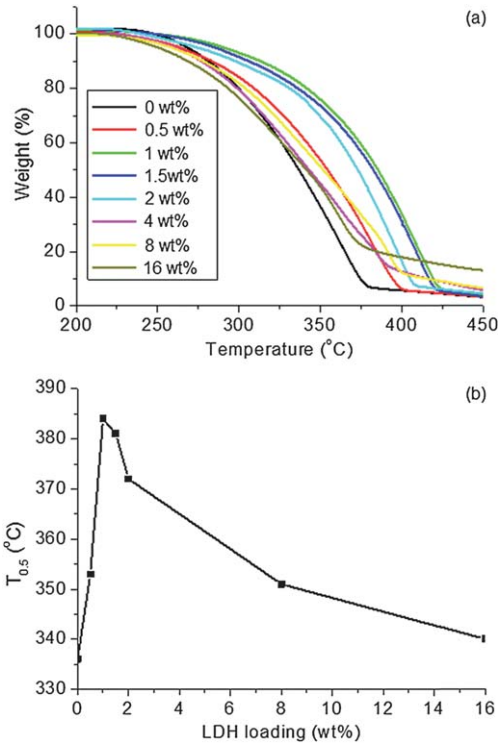

Fig. 12 (a) Thermal stability of PP/Mg–Al–DDS LDH nanocomposites evaluated by TGA. (b) The 50% weight loss temperature ($T_{0.5}$) variation as a function of LDH loading in the PP/Mg–Al–DDS LDH nanocomposite.

Table 1 Summary of the melting temperature (T_m), ΔH_c and the recrystallization temperature (T_c), ΔH_m and crystallinity fraction (X_c) as measured by DSC for the PP/Mg–Al–DDS nanocomposites

LDH loading (wt%)	T_c/°C	ΔH_c/J g^{-1}	T_m/°C	ΔH_m/J g^{-1}	X_c (%)
0	108.31	85.61	153.65	85.70	58.4
1.0	115.04	98.25	156.10	91.75	67.1
1.5	116.25	101.4	156.19	90.28	69.2
2.0	117.89	95.72	156.47	87.59	65.3
4.0	117.83	96.05	156.40	90.10	65.6
8.0	116.46	98.56	155.63	89.25	67.3
16.0	117.51	90.11	157.17	83.75	61.5

The rheological behavior of the nanocomposite melts is very important for industrial nanocomposite processing. Furthermore, the formation of a percolated system can be detected by characterising the complex viscosity (η^*), storage modulus (G'), and loss modulus (G'') as a function of frequency (w).[73–75] The storage and loss moduli of the pure PP and its nanocomposite melts containing the nanoplatelet LDHs from 0.5 to 16.0 wt% at 200 °C are presented in Fig. 13(a) and (b). Unlike many other fillers, these nanoLDH filled polymer nanocomposites showed decreased G' and G'' when the loading was low (<2.0 wt%). With 0–2.0 wt% of LDHs, both G' and G'' decreased with the increase of LDH loading. The reduced G' and G'' are attributed to the enhanced mobility (relaxation) of confined polymer chains at the interface of the PP–LDH layer, a similar phenomenon has been reported previously.[43,76] Such a relaxation behavior only exists in the nano-regime, which well explains the nanosize of the LDH

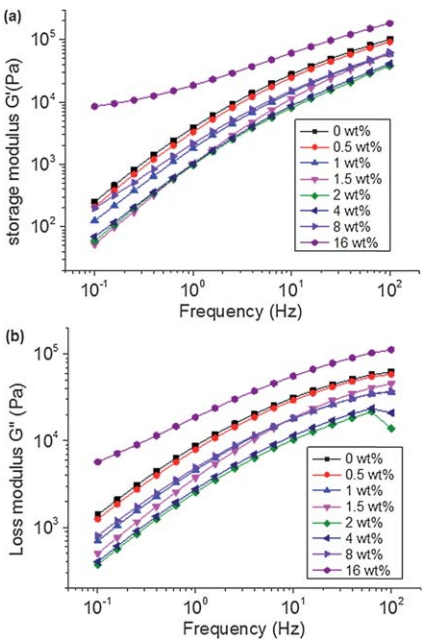

Fig. 13 (a) Storage modulus (G') and (b) loss modulus (G'') as a function of frequency for PP and PP/LDH nanocomposites.

in the nanocomposites.[77,78] The complex viscosity $\eta^*(w)$ is strongly related to G' and G'' and can be calculated using the following equation (eqn (2)). Therefore, the reduced viscosity is also observed in Fig. 14(b). However, increasing the LDH loading from 2.0 wt% to 16.0 wt% gradually increased both G' and G''. At a 16.0 wt% LDH loading, the rheological response changes and the elastic solid-like behavior is observed, with only a limited reduction in G' at low w.

$$\eta^*(\omega) = [(G'/\omega)^2 + (G''\omega)^2]^{1/2} \quad (2)$$

Fig. 14(a) shows the mechanical loss factor (tan δ) as a function of w. The tan δ, which arises from the discordance between strain and stress in the polymer exposed to an external force, is strongly related to applied frequency. For pure PP and its nanocomposites with 0.5–4.0 wt% LDHs, tan δ decreases monotonously with increasing w. While from 8.0 wt%, tan δ starts to show three different stages: rubbery, viscoelastic and a glassy state.[79] A minimum in tan δ is observed with 16.0 wt% LDH filled PP nanocomposites. When the LDH loading is low (0–1.5 wt%), tan δ increases with increasing loading, reaching a maximum value at 1.5 wt%. tan δ then decreases with the further increase of LDH loading from 1.5 wt% to 16.0 wt%. The incorporation of the LDH nanoparticles will restrain the relative motion of the polymer chain and makes the nanocomposites "stiffer".[80–82]

Fig. 14(b) shows the complex viscosity (η^*) as a function of w for the pure PP and its nanocomposites at 200 °C. η^* first decreased with increasing LDH loading up to 2.0 wt%, and then begins to increase with further increasing loading to 16.0 wt%. The pure PP shows a classical viscoelastic behavior characterised by a transition from low frequency Newtonian flow behaviour to high frequency shear thinning nature (viscosity decreases with an increase of shear rate/frequency).[82–84] Similar fluid properties were observed in the PP/LDH nanocomposites with the LDH loading up to 8.0 wt%. However, as the LDH loading is increased up to 16.0 wt %, the viscosity curve becomes linear within the whole frequency range. This phenomenon indicates the filler dominated fluid in the nanocomposites with a relatively high particle loading. The transition in η^* indicates that the nanocomposites have reached a rheological percolation, at which the nanoparticles form a network structure and greatly impede the motion of the polymer chains.[85]

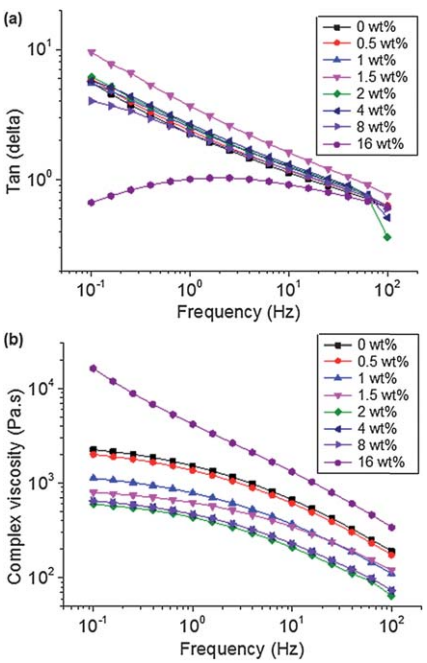

Fig. 14 Variation in tan δ and complex viscosity as a function of frequency for PP and PP/LDH nanocomposites.

4 Conclusions

We report a simple one step synthesis of PP/LDH nanocomposites. The method produces an excellent dispersion of nanoplatelet LDHs in the PP. The microemulsion method also produces nanoplatelets with an interlamellar distance of 30 Å and with a narrow lateral width dimensions of *ca.* 50 nm. The particle size of the nanocomposites decreases with the increase of LDH loadings, suggesting that the LDH nanosheets work as the nucleation seed during the rapid precipitation of the nanocomposites. The excellent dispersion of the LDH nanosheets within the PP matrix is indicative of an excellent compatibility of the hydrophilic LDH nanoplatelets with the PP matrix. We have found that adding the LDH greatly enhances the thermal stability of the PP, with an increase of 48 °C in $T_{0.5}$ of 1.0 wt% loading. The nanoplatelet LDHs also increase the melting and the recrystallisation temperatures of the nanocomposites compared to the pure PP. Rheological studies demonstrated that the G', G'', tan δ, and η^* of PP can be tuned by adding specific amounts of these dispersed LDHs.

Acknowledgements

The authors thank SCG Chemicals, Thailand for financial support. Z. Guo appreciates the support from NSF (CMMI 10-30755).

Notes and references

1 P. Ding, M. Zhang, J. Gai and B. Qu, *J. Mater. Chem.*, 2007, **17**, 1117.
2 S. O'Leary, D. O'Hare and G. Seeley, *Chem. Commun.*, 2002, 1506.
3 F. Leroux and C. T. Gueho, *J. Mater. Chem.*, 2005, **15**, 3628.
4 M. C. Nshuti, D. Y. Wang, J. M. Hossenlopp and C. A. Wilkie, *J. Mater. Chem.*, 2008, **18**, 3091.
5 C. Taviot-Gueho and F. Leroux, *Struct. Bonding*, 2006, **119**, 121.
6 Q. Wang and D. O'Hare, *Chem. Rev.*, 2012, **112**, 4124.
7 E. R. Hitzky, M. Darder and P. Aranda, *J. Mater. Chem.*, 2005, **15**, 3650.
8 P. B. Messersmith and S. I. Stupp, *Chem. Mater.*, 1995, **7**, 454.
9 M. Darder, P. Aranda and E. R. Hitzky, *Adv. Mater.*, 2007, **19**, 1309.
10 M. M. E. Jacob, E. Hackett and E. P. Giannelis, *J. Mater. Chem.*, 2003, **13**, 1.
11 H. B. Hsueh and C. Y. Chen, *Polymer*, 2003, **44**, 5275.
12 W. D. Lee, S. S. Im, H. M. Lim and K. J. Kim, *Polymer*, 2006, **47**, 1364.
13 F. Leroux, J. Gachon and J. P. Besse, *J. Solid State Chem.*, 2004, **177**, 245.
14 P. J. Purohit, J. E. Huacuja-Sanchez, D. Y. Wang, F. Emmerling, A. Thunemann, G. Heinrich and A. Schonhals, *Macromolecules*, 2011, **44**, 4342.
15 F. R. Costa, U. Wagenknecht, D. Jehnichen, M. A. Goad and G. Heinrich, *Polymer*, 2006, **47**, 1649.
16 Q. Wang, X. Zhang, J. Zhu, Z. Guo and D. O'Hare, *Chem. Commun.*, 2012, **48**, 7450.

17 M. Zhang, P. Ding and B. Qu, *Polym. Compos.*, 2009, **30**, 1000.
18 D. Y. Wang, A. Das, F. R. Costa, A. Leuteritz, Y. Z. Wang, U. Wagenknecht and G. Heinrich, *Langmuir*, 2010, **26**, 14162.
19 F. R. Costa, U. Wagenknecht and G. Heinrich, *Polym. Degrad. Stab.*, 2007, **92**, 1813.
20 W. Chen and B. Qu, *J. Mater. Chem.*, 2004, **14**, 1705.
21 P. Ding and B. J. Qu, *J. Polym. Sci., Part B: Polym. Phys.*, 2006, **44**, 3165.
22 C. Manzi-Nshuti, J. M. Hossenlopp and C. A. Wilkie, *Polym. Degrad. Stab.*, 2008, **93**, 1855.
23 W. Chen, L. Feng and B. Qu, *J. Solid State Commun.*, 2004, **130**, 259.
24 Y. J. Lin, D. Q. Li, D. G. Evans and X. Duan, *Polym. Degrad. Stab.*, 2005, **88**, 286.
25 Z. P. Xu, S. K. Saha, P. S. Braterman and N. D'Souza, *Polym. Degrad. Stab.*, 2006, **91**, 3237.
26 S. Yi, Z. H. Yang, S. W. Wang, D. R. Liu, S. Q. Wang, Q. Y. Liu and W. W. Chi, *J. Appl. Polym. Sci.*, 2011, **119**, 2620.
27 H. Zhu, W. Wang and T. Liu, *J. Appl. Polym. Sci.*, 2011, **122**, 273.
28 B. Sahu and G. Pugazhenthi, *J. Appl. Polym. Sci.*, 2011, **120**, 2485.
29 C. Nyambo and C. A. Wilkie, *Polym. Degrad. Stab.*, 2009, **94**, 506.
30 D. Y. Wang, A. Leuteritz, Y. Z. Wang, U. Wagenknecht and G. Heinrich, *Polym. Degrad. Stab.*, 2010, **95**, 2474.
31 H. Peng, W. C. Tjiu, L. Shen, S. Huang, C. He and T. Liu, *Compos. Sci. Technol.*, 2009, **69**, 991.
32 J. Ahn, M. Han and C. S. Ha, *Polym. Int.*, 2011, **60**, 271.
33 M. Zammarano, M. Franceschi, S. Bellayer, J. W. Gilmana and S. Meriani, *Polymer*, 2005, **46**, 9314.
34 L. Du, B. Qu, Y. Meng and Q. Zhu, *Compos. Sci. Technol.*, 2006, **66**, 913.
35 L. Du, B. Qu and M. Zhang, *Polym. Degrad. Stab.*, 2007, **92**, 497.
36 G. A. Bubniak, W. H. Schreiner, N. Mattoso and F. Wypych, *Langmuir*, 2002, **18**, 5967.
37 W. Chen and B. Qu, *Polym. Degrad. Stab.*, 2005, **90**, 162.
38 E. M. Moujahid, J.-P. Besse and F. Leroux, *J. Mater. Chem.*, 2003, **13**, 258.
39 J. Kaspersma, C. Doumen, S. Munro and A. M. Prins, *Polym. Degrad. Stab.*, 2002, **77**, 325.
40 L. Wang, X. He, H. Lu, J. Feng, X. Xie, S. Su and C. A. Wilkie, *Polym. Adv. Technol.*, 2011, **22**, 1131.
41 T. Kuila, H. Acharya, S. K. Srivastava and A. K. Bholomica, *J. Appl. Polym. Sci.*, 2008, **108**, 1329.
42 M. Darder, M. Blanco, P. Aranda, F. Leroux and E. R. Hitzky, *Chem. Mater.*, 2005, **17**, 1969.
43 F. R. Costa, M. Saphiannikova, U. Wagenknecht and G. Heinrich, *Adv. Polym. Sci.*, 2008, **210**, 101.
44 A.-L. Troutier-Thuilliez, C. Taviot-Guého, J. Cellier, H. Hintze-Bruening and F. Leroux, *Prog. Org. Coat.*, 2009, **64**, 182.
45 G. Hu, N. Wang, D. O'Hare and J. Davis, *J. Mater. Chem.*, 2007, **17**, 2257.
46 M.-P. Pileni, *Nat. Mater.*, 2003, **2**, 145.
47 M. Li, H. Schnablegger and S. Mann, *Nature*, 1999, **402**, 393.
48 D. Walsh, J. D. Hopwood and S. Mann, *Science*, 1994, **264**, 1576.
49 T. Dwars, E. Paetzold and G. Oehme, *Angew. Chem., Int. Ed.*, 2005, **44**, 7174.
50 G. Hu and D. O'Hare, *J. Am. Chem. Soc.*, 2005, **127**, 17808.
51 G. Hu, N. Wang, D. O'Hare and J. Davis, *Chem. Commun.*, 2006, 287.
52 C. J. Wang, Y. A. Wu, R. M. J. Jacobs, J. H. Warner, G. R. Williams and D. O'Hare, *Chem. Mater.*, 2011, **23**, 171.
53 M. E. Perez-Bernal, R. J. Ruano-Casero, F. Benito and V. Rives, *J. Solid State Chem.*, 2009, **182**, 1593.
54 A. Wongariyakawee, F. Schaeffel, J. H. Warner and D. O'Hare, *J. Mater. Chem.*, 2012, **22**, 7751.
55 H. Wu, Q. Jiao, Y. Zhao, S. Huang, X. Li, H. Liu and M. Zhou, *Mater. Charact.*, 2010, **61**, 227.
56 S. Wei, R. Patil, L. Sun, N. Haldolaarachchige, X. Chen, D. P. Young and Z. Guo, *Macromol. Mater. Eng.*, 2011, **296**, 850.
57 Y. Li, J. Zhu, S. Wei, J. Ryu, Q. Wang, L. Sun and Z. Guo, *Macromol. Chem. Phys.*, 2011, **212**, 2429.
58 M. M. J. Treacy, M. W. Deem and J. M. Newsam, *Computer Code DIFFaX, Version 1.807*.
59 W. Kagunya, R. Baddour-Hadjean, F. Kooli and W. Jones, *Chem. Phys.*, 1998, **236**, 225.
60 Z. P. Xu and G. Q. Lu, *Chem. Mater.*, 2005, **17**, 1055.
61 Q. Wang, Z. Wu, H. H. Tay, L. Chen, Y. Liu, J. Chang, Z. Zhong, J. Luo and A. Borgna, *Catal. Today*, 2011, **164**, 198.
62 P. Gunawan and R. Xu, *J. Mater. Chem.*, 2008, **18**, 2112.
63 Z. P. Xu and P. S. Braterman, *J. Mater. Chem.*, 2003, **13**, 167.
64 T. Hibino and W. Jones, *J. Mater. Chem.*, 2001, **11**, 1321.
65 P. Maiti, P. H. Nam, M. Okamoto, N. Hasegawa and A. Usuki, *Macromolecules*, 2002, **35**, 2042.
66 Y. Shi, S. Peterson and D. Y. Sogah, *Chem. Mater.*, 2007, **19**, 1552.
67 B. N. Jang and C. A. Wilkie, *Polymer*, 2005, **46**, 2933.
68 K. T. Gilman and T. Kashiwagi, *Polymer/Clay Nanocomposites*, ed. T. J. Pinnavaia and G. W. Beall, John Wiley & Sons, New York, 2000, p. 193.
69 J. Zhu and C. A. Wilkie, *Polym. Int.*, 2000, **49**, 1158.
70 J. Zhu, F. M. Uhl, A. B. Morgan and C. A. Wilkie, *Chem. Mater.*, 2001, **13**, 4649.
71 S. P. Lonkar, S. Morlat-Therias, N. Caperaa, F. Leroux, J. L. Gardette and R. P. Singh, *Polymer*, 2009, **50**, 1505.
72 M. Eder and A. Wlochowicz, *Polymer*, 1983, **24**, 1593.
73 J. Zhu, S. Wei, J. Ryu, M. Budhathoki, G. Liang and Z. Guo, *J. Mater. Chem.*, 2010, **20**, 4937.
74 J. Zhu, S. Wei, A. Yadav and Z. Guo, *Polymer*, 2010, **51**, 2643.
75 C. A. Mitchell, J. L. Bahr, S. Arepalli, J. M. Tour and R. Krishnamoorti, *Macromolecules*, 2002, **35**, 8825.
76 G. Barut, P. Pissis, R. Pelster and G. Nimtz, *Phys. Rev. Lett.*, 1998, **80**, 3543.
77 A. Huwe, F. Kremer, P. Behrens and W. Schwieger, *Phys. Rev. Lett.*, 1999, **82**, 2338.
78 J. Baschnagel, C. Mischler and K. Binder, *J. Phys. IV*, 2000, **10**, 7.
79 G. Schramm, *A Practical Approach to Rheology and Rheometry*, Gebrueder HAAKE GmbH, Karlsruhe, Federal Republic Germany, 2nd edn, 2000.
80 Y. Li, J. Zhu, S. Wei, J. Ryu, L. Sun and Z. Guo, *Macromol. Chem. Phys.*, 2011, **212**, 1951.
81 X. Chen, S. Wei, A. Yadav, R. Patil, J. Zhu, R. Ximenes, L. Sun and Z. Guo, *Macromol. Mater. Eng.*, 2011, **296**, 434.
82 J. Zhu, S. Wei, Y. Li, L. Sun, N. Haldolaarachchige, D. P. Young, C. Southworth, A. Khasanov, Z. Luo and Z. Guo, *Macromolecules*, 2011, **44**, 4382.
83 A. J. Poslinski, M. E. Ryan, R. K. Gupta, S. G. Seshadri and F. J. Frechette, *J. Rheol.*, 1988, **32**, 703.
84 V. M. Ugaz, D. K. Cinader and W. R. Burghardt, *Macromolecules*, 1997, **30**, 1527.
85 A. V. Shenoy, *Rheology of Filled Polymer Systems*, Kluwer Academic Publishers, Dordrecht, The Netherlands, 1999.